DOI: 10.1002/asia.200800160

# Tartardiamide-Functionalized Chiral Organosilicas with Highly Ordered Mesoporous Structure

Lei Zhang,[a] Jian Liu,[a, b] Jie Yang,[a] Qihua Yang,*[a] and Can Li*[a]

**Abstract:** A novel chiral mesoporous organosilica with L-tartardiamide moieties integrated in the backbone has been synthesized for the first time by a mild synthetic approach with block copolymer P123 as a template. The materials have highly ordered 2D hexagonal mesostructure and uniform pore size in the range of 7.6 to 5.5 nm. NMR, IR, and TG analyses confirm that the tartardiamide group was successfully incorporated into the framework. The intrinsic chirality of L-tartardiamide endows the materials with unique optical activities and chiral-recognition properties. By dissolving the materials into NaOH, the solutions show rotation of polarized light by +8.42° to +15.53°, depending on the amount of the chiral moieties in the materials. Owing to the chirality of L-tartardiamide, the materials exhibited chiral-induction ability in the epoxidation of allyl alcohol, thus further demonstrating the chirality of the materials.

**Keywords:** chirality · L-tartardiamide · mesoporous materials · organic–inorganic hybrid composites · template synthesis

## Introduction

The design and synthesis of novel solid chiral materials, especially organic–inorganic hybrid chiral materials, have continued to be an area of extensive interest, because these materials have enormous and important applications in asymmetric catalysis,[1,2] chiral separation, sequestration, and chromatography,[3,4] for obtaining enantiopure chemicals and pharmaceuticals. Moreover, they may also exhibit nonlinear optical effects, piezoelectricity, and pyroelectricity, which are technologically important for the development of polarizer-sensitive electrooptical devices.[5] It has been recognized that such properties and potential applications depend not only on the structure of the building units, but also largely on the building process.

Recent developments of ordered mesoporous materials have enabled one to control the pore structure and the dispersion of the active components on the nanometer scale.[6–8] Introduction of uniform and ordered mesopores in solid chiral materials will enhance the accessibility of the active sites, provide easier inclusion of guest species, and allow for further modification of the materials and fine-tuning of the host–guest interactions towards specific demands. Among the various hybrid mesoporous materials reported so far, periodic mesoporous organosilicas (PMOs) present one of the most important innovations.[9–11] With bridged organosilane $(R'O)_3$-Si-R-Si-$(OR')_3$ as the precursor, PMOs feature highly porous structures and organic–inorganic backbones hybridized at the molecular scale. The organic groups are covalently bonded and homogeneously distributed throughout the framework. Thus, by altering the type and content of the bridging organic groups, the chemical/physical properties of both the pore surface and the framework can be tuned. To date, numerous organic groups have been incorporated into PMOs, including small aliphatic and aromatic groups,[12,13] even some ferrocene,[14] cyclam,[15] dendrimer,[16] and cubic oligomer compounds.[17] Specifically, incorporating chiral moieties into PMOs has given rise to a new family of promising solid chiral materials.[18–21]

Although chiral PMOs have already been proposed in 1999 shortly after the discovery of PMOs,[18] the report of chiral PMOs built exclusively with chiral blocks did not emerge until 2006.[19] This is due to the difficulties in the

[a] L. Zhang, J. Liu, J. Yang, Prof. Dr. Q. Yang, Prof. Dr. C. Li
State Key Laboratory of Catalysis
Dalian Institute of Chemical Physics, Chinese Academy of Sciences
457 Zhongshan Road, Dalian 116023 (China)
Fax: (+86) 411-84694447
E-mail: yangqh@dicp.ac.cn
canli@dicp.ac.cn

[b] J. Liu
Graduate School of the Chinese Academy of Sciences
Beijing 100039 (China)

Supporting information for this article is available on the WWW under http://dx.doi.org/10.1002/asia.200800160.

synthesis and purification of enantiomerically pure chiral organosilanes suitable for the synthesis of PMOs. Polarz and Kuschel reported the first chiral PMOs with the framework composition of $[O_{1.5}SiCH_2C^*H(OH)SiO_{1.5}]$ from a boron-ester-protected chiral silane.[19] However, owing to the harsh basic synthesis conditions, some Si–C bonds were cleaved. Moreover, no information about the chirality of the final material was given. Also starting from a hydroborated chiral silane, Thomas et al. reported the synthesis of chiral amine-functionalized mesoporous organosilicas by post-ammonolysis.[20] More recently, Inagaki et al. reported the synthesis of (*R*)-(+)-phenylethylene-bridged chiral microporous organosilicas and characterized the chirality of the materials after dissolution by HF.[21] However, the above-mentioned chiral PMOs still lack the necessary functionalities to be ready for practical applications. Moreover, it is difficult to build ordered and rigid porous structures from 100% organosilanes owing to the steric hindrance of the chiral moieties on the assembly process.

In an alternative approach, organosilanes with bulky and flexible chiral moieties can be admixed with small silane compounds (e.g., tetraalkoxysilane) to generate ordered and rigid porous structures.[22–26] Corma et al. first reported the synthesis of chiral PMOs through the condensation of chiral vanadyl Schiff base complexes and tetraethoxysilane (TEOS).[22,23] In the cyanosilylation of benzaldehyde, the material gave 30% enantiomeric excess. García et al. reported chiral diaminocyclohexane- and binaphthyldiamine-derived chiral PMOs using a similar co-condensation method.[24] In the di-π-methane rearrangement of 11-formyl-12-methyldibenzobarrelene, an *ee* value of 24% was observed.[25] We have recently reported the synthesis of diaminocyclohexane-derived mesoporous organosilicas.[26] After complexation with a Rh complex, the material exhibited up to 30% *ee* for the asymmetric transfer hydrogenation of acetophenone. These chiral organosilanes have been based only on cyclohexadiyl or binaphthyl derivatives; therefore abundant chiral blocks still remain to be explored for the synthesis novel chiral mesoporous organosilicas.

**Abstract in Chinese:**

*固体手性材料在多相不对称催化，手性拆分，手性识别以及非线性光学材料等方面都具有广泛的应用前景。设计并合成具有特定结构和功能的新型固体手性材料是实现这些应用的基础。本文介绍了一种新型的固体手性介孔材料—酒石酸酰胺功能化的有机－无机杂化介孔材料的合成。通过采用温和的合成条件，在酒石酸酰胺的结构保持的同时，得到了具有高度有序介观结构及均匀孔径（7.6－5.5 nm）的杂化材料。由于酒石酸酰胺的手性特性，材料溶解在 NaOH 水溶液后表现出一定的旋光活性（+8.42° － +15.53°）。该材料与 Ti 配位后，在丙烯醇的环氧化反应中表现出一定的手性诱导能力（～20% ee），进一步表明了材料的手性特征。*

In contrast to the ever-expanding composition of chiral mesoporous organosilicas, the synthetic approach to such materials has been mostly conducted under strongly basic conditions with an alkylammonium surfactant as the template.[19,21–26] In most cases, the pore size is restricted to 3 nm, and the structural regularity is remarkably affected by the amount of the bulky chiral bridging organosilanes. Moreover, since many chiral species are prone to decomposition or racemization under harsh acidic or basic conditions,[19,21] a mild synthetic method for chiral mesoporous organosilicas is highly desirable. Poly(ethylene oxide)-poly(propylene oxide)-poly(ethylene oxide) (PEO-PPO-PEO) block copolymers, such as P123 and F127, have been successfully utilized as the template for the synthesis of mesoporous silicas and organosilicas with pore sizes larger than 6 nm.[27] More importantly, with block copolymer P123 as the template, mesoporous materials can be synthesized under a wide range of pH values,[28,29] which provides more opportunities for the synthesis of chiral PMOs under mild conditions. However, to the best of our knowledge, no chiral PMOs with highly ordered large mesopores have been synthesized with a block copolymer as the template.

Among the various chiral blocks, tartaric acid and its derivatives represent one of the earliest discovered, most extensively investigated and versatile families of chiral compounds. Tartaric derivatives have been widely used in optical devices,[30] asymmetric catalysis as ligands or modifiers,[31–34] and chiral separation.[35,36] Integration of abundant chiral tartaric derivatives into mesoporous materials will generate a brand new group of chiral materials with potential chirality-revelant applications. Herein, we report the first synthesis of highly ordered large pore mesoporous organosilicas with L-tartardiamide in the framework. A mild synthetic approach was employed with block polymer P123 as the template under weakly acidic conditions (Scheme 1). The materials show optical activity by rotating the plane of polarized light by a specific angle after being dissolved in NaOH solution. Moreover, in the epoxidation of allyl alcohol the materials show moderate chiral-induction ability.

## Results and Discussion

### Synthesis and Structural Characterization of Tartardiamide-Containing Chiral Mesoporous Organosilicas (TarMOs)

The chiral block used in this study is L-tartardiamide-bridged organosilane **1** (Scheme 1). Control experiments showed that under highly acidic conditions (2.0 M HCl aqueous solution) or basic synthesis conditions, decomposition of compound **1** occurred during the synthesis (see the Supporting Information for details). Since the amide bond in **1** is labile under highly basic or acidic conditions, to preserve the chiral structure during the preparation, we attempted to conduct the synthesis under mild conditions. Block copolymer P123 was used as a template because it presents several advantages. Poly(ethylene oxide) block copolymers can be more easily extracted from the pore channels than the ionic

  

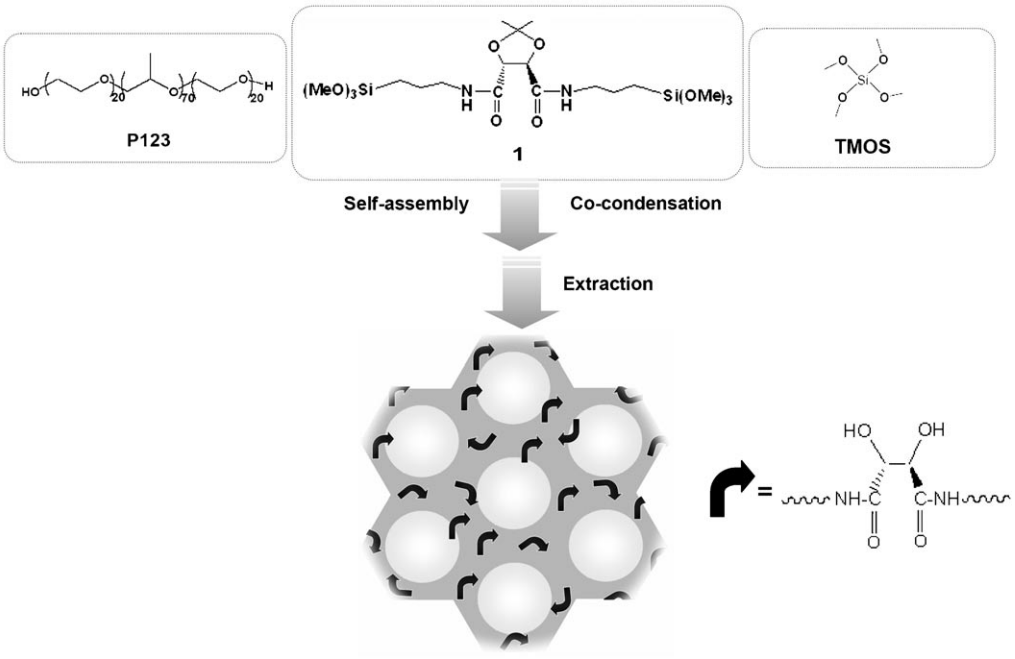


Scheme 1. Synthetic approach toward chiral mesoporous organosilicas with L-tartardiamide in the framework.

surfactants which have been frequently used in the syntheses of chiral PMOs.[19,21–26] The materials templated by P123 have additional framework micropores interconnecting the primary large mesopores into a 3D porous structure, which is beneficial for the adsorption and diffusion of guest molecules. More importantly, P123 can direct the formation of ordered mesostructure under a wide range of pH values, even under near-neutral conditions,[29,37] which is important for the preservation of reactive organic functionalities during the synthesis. Sodium chloride was used as an additive to increase the structural regularity because the salting-out effect can enhance the assembly ability of micelles.[38] Samples thus obtained are denoted as TarMO-*x*, abbreviated from tartardiamide-containing mesoporous organosilica, wherein $x = [\mathbf{1}/(\mathbf{1}+\mathrm{TMOS})] \times 100$ (TMOS = tetramethoxysilane; compounds in equation represent molar equivalents), representing the molar percent of **1** in the silane mixture.

Kim et al. reported that pure mesoporous silica with a highly ordered mesostructure could be synthesized under neutral condition with fluoride as the hydrolysis catalyst.[29] We first prepared TarMOs under neutral conditions ([HCl] = 0 M) using $F^-$ as the hydrolysis–condensation catalyst. However, only disordered materials were obtained after the removal of the template, as evidenced by the featureless XRD pattern (Figure 1). As will be discussed below, these may be due to the weak interactions between the silica oligomers (especially the organosilica oligomers) and the template molecules under neutral conditions, as well as the perturbation of the long-chain silane **1** on the assembly process.

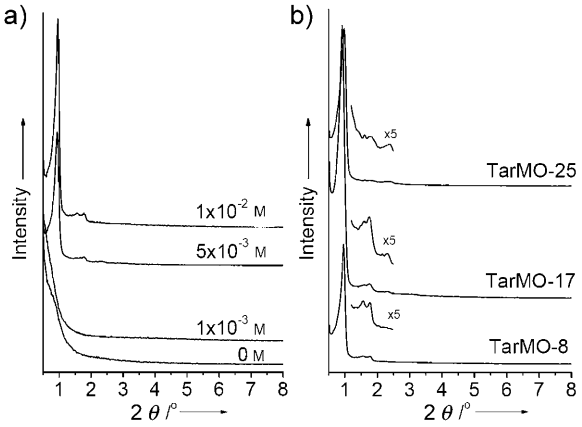


Figure 1. a) XRD patterns of chiral mesoporous organosilicas TarMO-8 synthesized with different HCl concentrations; b) TarMO-*x* samples with varying tartardiamide content synthesized with $1 \times 10^{-2}$ M HCl.

For mesoporous silica synthesized with PEO-PPO-PEO type block copolymers as the template, the assembly process is driven by the interaction between the hydrophilic PEO chain of P123 and the silica oligomers. Under neutral conditions, a hydrogen-bond-driven assembly is proposed ($N^0I^0$),[39] while under acidic conditions an anion-mediated assembly is proposed ($S^0H^+X^-I^+$).[28] The perturbation of **1** on the assembly process may arise from several aspects. First, the hydrophobic bridging organic group may interfere with the interface assembly between the PEO chains and the silica and break the structure of the micelle. Second, owing to the presence of the bridging organic groups, the

  

density of the effective interaction sites of the organosilica oligomers (≡SiOH or ≡SiO$^-$) in a given dimension is significantly lowered compared with that of the silica oligomers, which is detrimental to the silica–template interface interaction. Third, the long bridging organic group in silane **1** can exert strong steric hindrance and retard the hydrolysis and condensation rates of **1**, further reducing the density of ≡SiOH or ≡SiO$^-$ sites. We then introduced HCl into the synthesis medium to strengthen the interaction between the organosilica and the PEO corona of the P123 micelles. To keep the structure and configuration of **1** intact, we increased the concentration of the HCl solution gradually to find the lowest acid amount necessary for obtaining a highly ordered mesostructure. Figure 1a shows the XRD patterns of TarMO-8 samples [**1**/(**1**+TMOS)=8%] synthesized with different HCl concentrations after the extraction of the template. When the HCl concentration was $1\times10^{-3}$ M, the as-synthesized sample showed a very broad peak at low diffraction angle, indicative of short-range ordering (data not shown). However, the diffraction peak disappeared after the template was removed, suggesting that the pore structure collapsed after the relief of the template. When the concentration of HCl was increased to $5\times10^{-3}$ M, the XRD pattern of the as-synthesized TarMO-8 sample showed a strong diffraction with a broad shoulder. After the template extraction, the intensity of the first peak was greatly enhanced, indicating the preservation of the mesostructure. Upon further increasing the HCl concentration to $1\times10^{-2}$ M, the XRD pattern of the extracted sample showed three distinct peaks which could be readily indexed to (100), (110), and (200) peaks of a highly ordered *P6mm* mesophase. As will be shown below, the tartardiamide bonds were preserved in the materials synthesized with $1\times10^{-2}$ M HCl. We thus synthesized TarMO materials with a higher loading of **1** (17% and 25%) at a HCl concentration of $1\times10^{-2}$ M.

Figure 1b displays the XRD patterns of the extracted TarMO-*x* with different loadings of **1** ($x=[\mathbf{1}/(\mathbf{1}+\text{TMOS})]\times100$) . When *x* reaches 25, the intensities of the (110) and (200) peaks become lower and less resolved for TarMO-25 compared with those of TarMO-8 and TarMO-17. This may be due to the weakened interaction between the silica/organosilica oligomers and the PEO corona of P123 induced by the increased amount of the organic bridging group and the reduced density of silanol groups at the silica–template interface. Also, the flexibility of **1** renders the framework less rigid and lowers the pore regularity. Nevertheless, the periodicity of TarMO-25 is still comparatively high for chiral mesoporous organosilicas reported so far, taking into account the high content of bridged organosilane **1** (25% based on the silane molar ratio and 40% based on the silicon atom molar ratio). Interestingly, the peak intensity ratio of (110)/(200) for TarMO-*x* samples is smaller than those of most SBA-15 materials. Previous reports showed that the intensity of peak (110) was related to the degree of framework condensation.[40–43] Zhao et al. also observed this phenomenon for the ethylene-bridged PMOs[43] and ascribed it to the rapid condensation of organosilica around the micelles, which resulted in poorly defined pores. Based on previous studies and the structure of **1**, we suggest that the large bridging organic groups occluded inside the pore walls disturb the condensation of the framework, which results in a lower degree of condensation and hence reduces the scattering intensity of the (110) peak. Moreover, the organic groups in the framework have intrinsic scattering intensity different from that of silica, which could also affect the scattering intensity contrast. Figure 2 shows the TEM images of

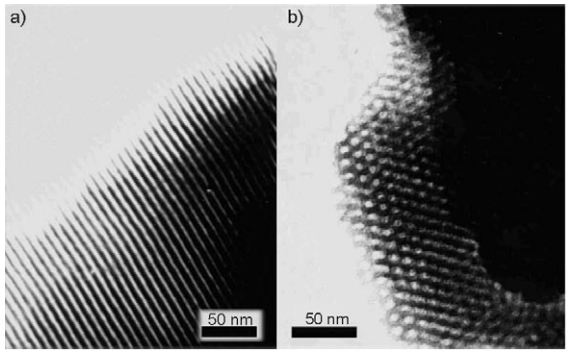


Figure 2. TEM images of sample TarMO-17 with the incidence direction a) perpendicular to the pore axis and b) parallel to the pore axis.

TarMO-17. Honeycomb structure as well as parallel fringe structure can be observed with the incidence direction parallel and perpendicular to the pore axis, respectively. This confirms that TarMO-17 has a highly ordered *P6mm* phase.[28] The results shown above indicate that highly ordered chiral PMOs with high tartardiamide content can be synthesized under mild acidic conditions.

Figure 3 shows the nitrogen sorption isotherms and the corresponding pore size distribution curves of TarMO-*x* samples synthesized with $1\times10^{-2}$ M HCl. All three samples exhibit typical IV isotherms with H1 hysteresis loops in the relative pressure $P/P_0$ range of 0.5 to 0.8, which is character-

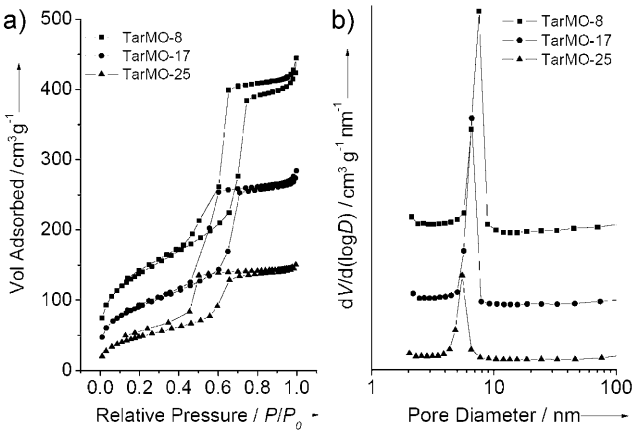


Figure 3. a) Nitrogen sorption isotherms and b) pore size distribution curves of TarMO-*x* samples with different tartardiamide contents synthesized with $1\times10^{-2}$ M HCl. All data were collected at STP.

  

istic of mesoporous materials with large mesopores.[28] The steepness of the hysteresis reflects the pore size uniformity of the three samples. Increasing of the amount of **1** induces a gradual decrease in the BJH pore size from 7.6 to 5.5 nm, BET surface area from 498 to 180 $m^2 g^{-1}$, and total pore volume from 0.65 to 0.22 $cm^3 g^{-1}$ (Table 1). Considering the flexibility of **1**, the higher amount of **1** incorporated, the less rigid the framework will be. After the removal of the template, the pore may shrink and cause a decrease in the primary mesopore surface area ($S_p$) and the mesopore volume ($V_p$, Table 1). Moreover, upon increasing the content of **1** in the framework, the micropore surface area ($S_{mic}$) and micropore volume ($V_{mic}$) dropped gradually. The generation of micropores inside the pore walls of SBA-15 type materials has been attributed to the penetration of the copolymer template into the silica framework during the assembly process.[41] The decrease in micropores could be ascribed to the enhanced hydrophobicity and lowered silanol density in the framework, which would weaken the interaction of the pore wall with the template.

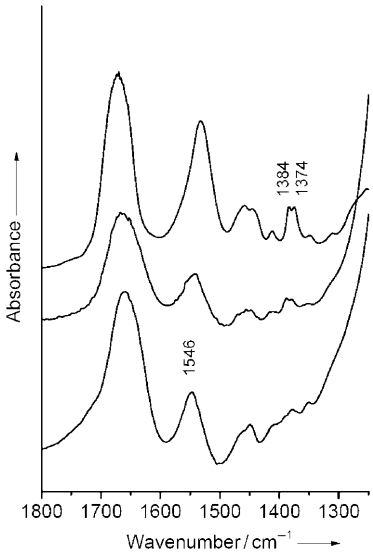


Figure 4. IR spectra of compound **1** (top curve), SBA-15 grafted with **1** (middle), and sample TarMO-8 synthesized with $1\times10^{-2}$ M HCl (bottom).

### Composition Characterization of TarMOs

Figure 4 shows the IR spectrum of TarMO-8 synthesized with $1\times10^{-2}$ M HCl. For comparison, the spectra of compound **1** and a SBA-15 sample grafted with **1** are also shown. TarMO-8 gives a similar spectrum to that of the SBA-15 grafted with **1**, implying the preservation of integrity of the organic groups during the synthesis. A band resulting from the coupling of $\nu_{C\text{-}N}$ with $\delta_{N\text{-}H}$ vibrations of amide bonds appears at 1546 $cm^{-1}$. No peak corresponding to carboxyl (ca. 1710 $cm^{-1}$) was observed for TarMO-8, indicating that no amide bonds were hydrolyzed during the synthesis. The band at 1664 $cm^{-1}$ arising from the $\nu_{C=O}$ mode is overlapped with the peak of adsorbed water. For compound **1** and the grafted sample, the double peaks at 1374 and 1384 $cm^{-1}$ with comparable intensity are characteristic of the isopropyl group in **1**. For sample TarMO-8, however, the peak intensity at 1384 $cm^{-1}$ is remarkably lower than that of 1374 $cm^{-1}$, indicating partial detachment of the protecting isopropyl group during the synthesis.

To further confirm the incorporation of the tartardiamide moieties in TarMOs, $^{29}$Si MAS NMR and $^{13}$C CP-MAS NMR were performed. $^{29}$Si MAS NMR data of TarMO-17 shows both the T and Q silicon sites (Figure 5a). The signals at $\delta=-108.8$, $-100.0$, and $-91.0$ ppm arise from the Si species $Q^4$ [$Si(OSi)_4$], $Q^3$ [$Si(OH)(OSi)_3$], and $Q^2$ [$Si(OH)_2(OSi)_2$], respectively. The signals at $-64.5$ and $-57.8$ ppm can be ascribed to the organosilicon species $T^3$ [$SiC(OSi)_3$] and $T^2$ [$SiC(OH)(OSi)_2$], respectively. The absence of a $T^0$ [$SiC(OH)_3$] site indicates that the chiral moiety is actually integrated with both ends in the pore walls, instead of dangling in the pore as a pendant group. Integration results show a peak area ratio of $\Sigma S_T/(\Sigma S_T+\Sigma S_Q)\approx28.3\%$, which agrees well with the initial precursor composition [$17\times2/(17\times2+83)\approx29.0\%$].

Figure 5b shows the $^{13}$C NMR data of TarMO-17. The signal at $\delta=173.5$ ppm can be ascribed to the carbonyl group (C=O, f). Signals at $\delta=42.3$, 22.6, and 9.8 ppm can be attributed to the propyl carbon atoms linked to the silicon atom (a, b, and c). The broad signals in the range of 70 to 80 ppm with a central peak around 73.0 ppm can be ascribed to the chiral carbon atoms (d, d′). According to the previous study,[32] the chiral carbon atom in **1** shows a signal in the range of 78 to 80 ppm, whereas the signals corresponding to

Table 1. Textural parameters of chiral mesoporous organosilicas with varying tartardiamide content synthesized with $1\times10^{-2}$ M HCl.

| Sample | $a_0$[a] [nm] | $S_{BET}$[b] [$m^2 g^{-1}$] | $S_{mic}$[b] [$m^2 g^{-1}$] | $S_p$[b] [$m^2 g^{-1}$] | $V_t$[c] [$cm^3 g^{-1}$] | $V_{mic}$[c] [$cm^3 g^{-1}$] | $V_p$[c] [$cm^3 g^{-1}$] | $D_p$[d] [nm] | $t_w$[e] [nm] | Tartardiamide content[f] [mmol $g^{-1}$] | $[\alpha]_D$[h] [°] |
|---|---|---|---|---|---|---|---|---|---|---|---|
| TarMO-8 | 10.6 | 498 | 146 | 316 | 0.65 | 0.062 | 0.51 | 7.6 | 3.0 | 0.60 (0.81)[g] | +8.42 |
| TarMO-17 | 11.1 | 329 | 71 | 238 | 0.42 | 0.029 | 0.35 | 6.5 | 4.6 | 0.93 (1.17)[g] | +12.34 |
| TarMO-25 | 10.4 | 180 | 20 | 146 | 0.22 | 0.005 | 0.19 | 5.5 | 4.9 | 1.24 (1.28)[g] | +15.53 |

[a] Unit cell parameter determined by ($d_{100}\times2/\sqrt{3}$). [b] $S_{BET}$ is the BET surface area. $S_{mic}$ and $S_p$ are the micropore surface area and the primary mesopore surface area, respectively, both determined by *t*-plot analysis. [c] $V_t$ is the total pore volume determined at relative pressure $P/P_0=0.99$. $V_{mic}$ and $V_p$ are the micropore volume and primary mesopore volume, respectively, both determined by *t*-plot analysis. [d] $D_p$ is the mesopore diameter determined from the adsorption branches of the $N_2$ sorption isotherms using the BJH method. [e] $t_w$ is the pore wall thickness determined by $a_0-D_p$. [f] The amounts of tartardiamide in the materials were determined by elemental analysis based on the N contents. [g] Numbers in parentheses are the tartardiamide content determined by TG analysis. [h] Determined by dissolving 0.05 g of sample in 10 mL of NaOH solution (1.0 M) at 10 °C; analysis conditions: JASCO P-1020, 5 s integration, 10 repeat times, 100 mm cell length.

  

CHEMISTRY
AN ASIAN JOURNAL

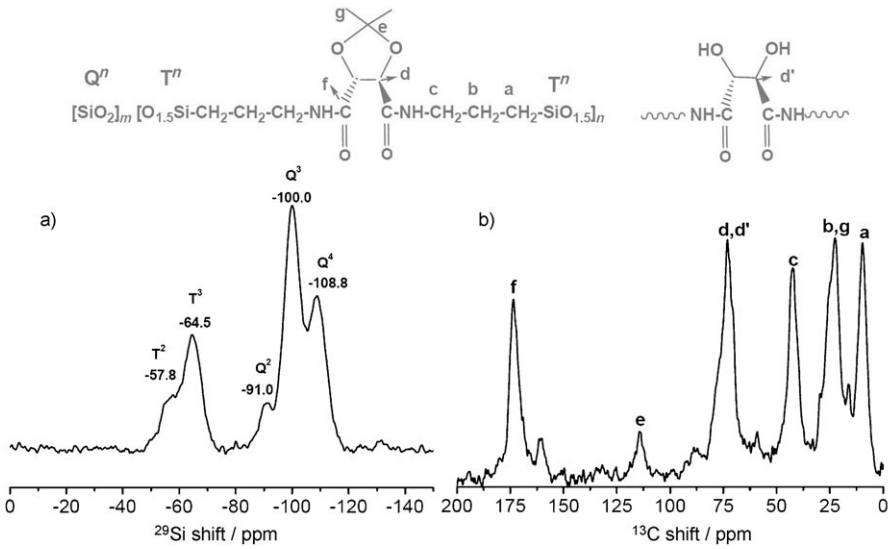


Figure 5. a) $^{29}$Si MAS NMR and b) $^{13}$C CP/MAS NMR spectra of sample TarMO-17.

this carbon atom shift to 70–73 ppm after the detachment of the isopropyl group. This indicates the partial removal of the protecting isopropyl group during the synthesis.[32] The presence of the small peak at 114 ppm corresponding to a quaternary carbon atom shows that some isopropyl groups are still present in the materials. After removal of the isopropyl group, the materials with chiral hydroxy groups may be useful as ligands in asymmetric catalysis as well as chiral discrimination and separation.[31–36] NMR data together with FTIR spectra confirm the successful incorporation of the tartardiamide group into the framework.

To determine the amount of the tartardiamide group incorporated into the resultant materials, thermogravimetric analysis (TGA) and elemental analysis (EA) were conducted on the TarMO-*x* samples. From the TGA profiles, two major steps of weight loss can be observed (Figure 6). Weight loss below 120 °C is due to the desorption of the physically adsorbed water and ethanol inside the pores. The

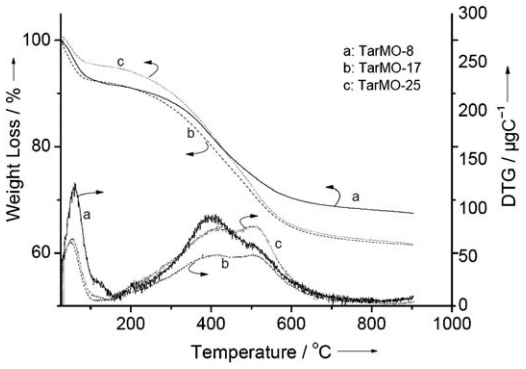


Figure 6. Thermogravimetric and differential thermogravimetric (DTG) profiles of TarMO-*x* samples with varying tartardiamide content synthesized with $1\times10^{-2}$ M HCl.

weight loss of TarMO-25 in this range is much lower than that of TarMO-8 and TarMO-17, which can be ascribed to the lower pore volume and enhanced surface hydrophobicity owing to the higher loading of organic groups. The weight loss from 200 to 600 °C arises from the decomposition of the framework organic groups and some remnant template. Weight loss in this temperature interval increases with the incremental loading of **1**. Weight loss from 600 °C can be ascribed to the further condensation of the framework and the surface silanols. The contents of the tartardiamide groups calculated from the TG results are shown in Table 1. Elemental analysis results based on the N atom content are also included. The incorporation amount of tartardiamide obtained by the TG profiles are higher than those from EA analysis, which may be caused by the remnant template in the materials.

### Characterization of the Chiral Properties of TarMOs

For solid chiral materials, one of the most important properties is their optical activity. Corma et al. evaluated the optical activity of VO(salen)-containing chiral PMOs by measuring the deviation angle of plane-polarized light using a conventional polarimeter of a suspension of the solid sample in 1,2-dichloroethane.[22] However, the inhomogeneity of the suspension may cause severe fluctuation of the measured deviation angle. We thus evaluated the chiral properties of TarMO-*x* samples indirectly by dissolving the material in 1.0 M NaOH at 10 °C (0.05 g of sample in 10 mL of NaOH solution). After the solution became clear, the deviation angle was measured in a polarimeter using the yellow Na emission at 25 °C. The NaOH solution (1.0 M) was used as the blank reference. As expected, all three samples rotated the plane of polarized light by a specific angle. The absolute rotation angle increases with the amount of tartardiamide (Table 1). However, it is difficult to establish quantitatively the relation between the rotation angle with the amount of chiral groups because the rotation angle can be affected by a number of factors, for example, the concentration of the chiral moiety, residual template, substitution alteration of the chiral center, and silica species in the solution, among others. Also, racemization of the chiral groups during the synthesis procedure can not be ruled out absolutely at present. Nevertheless, this indirect method does give qualitative evidence that TarMOs show optical activity by rotating the plane of polarized light and the activity increases with the

  

increment of the chiral groups in the materials. It would be interesting to fabricate transparent monolithic chiral PMOs and explore their applications in optical waveguides and nonlinear devices.

As the IR and NMR results show that most of the isopropyl groups were detached during the synthesis, the active hydroxyl groups connected to the chiral carbon atom become exposed and can interact with numerous guest molecules. To probe the accessibility and the potential chiral-recognition ability, the material was complexed with Ti and tested in the epoxidation of allyl alcohol (Scheme 2). All the hybrid materials show enantioselectivity with *ee* values up to 20%. Albeit lower than the optimal *ee* value of the heterogeneous catalyst synthesized by grafting methods under similar reaction conditions (80% *ee*),[32] this result demonstrates the chiral-recognition ability of the materials. Corma et al. also observed lower *ee* values for the VO(salen)-containing chiral PMOs than with the grafted counterpart.[22] This may be due to the fact that the configuration of chiral groups embedded in the framework is not appropriate to exert specific chiral induction needed for the epoxidation of allyl alcohol. On the other hand, the silanol groups may also coordinate with Ti and reduce the enantioselectivity. In view of catalysis applications, further work is needed to develop a more efficient synthesis approach to enhance the exposure and control the configuration of the stereogenic center.

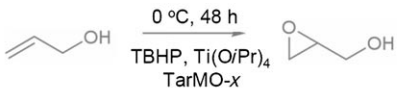


| Sample | Conversion [%] | *ee* [%] (*S*) |
|---|---|---|
| TarMO-8 | 24 | 19 |
| TarMO-17 | 46 | 20 |
| TarMO-25 | 40 | 15 |

Scheme 2. Epoxidation of allyl alcohol on chiral mesoporous organosilicas TarMO-*x* complexed with titanium. TBHP = *tert*-butyl hydroperoxide.

## Conclusions

We have synthesized a novel large-pore chiral mesoporous organosilica with L-tartardiamide integrated in the framework. Under mild synthetic conditions, a highly ordered mesostructure can be obtained while keeping the chiral bridging group intact. The resultant materials exhibit optical activity by rotating the plane of polarized light by a specific angle. Moreover, the materials show chiral inductivity in the epoxidation of allyl alcohol, thus further demonstrating the chiral nature of the materials. This work supplies the basis for research to optimize the synthetic conditions of chiral mesoporous organosilicas and exploit the chiral-recognition ability for asymmetric catalysis and chiral separation. With this mild synthetic approach, numerous novel chiral mesoporous organosilicas with highly ordered mesostructure are expected in the near future.

## Experimental Section

*Synthesis*

Silylated tartardiamide **1** (Scheme 1) was synthesized from L-(+)-tartaric acid according to a reported procedure,[32] except that 3-aminopropyltrimethoxysilane (Sigma–Aldrich) was used instead of 3-aminopropyltriethoxysilane.

Tartardiamide-containing chiral PMOs, denoted as TarMOs, were synthesized by the co-condensation of **1** and tetramethoxysilane (TMOS, Nanjing Shuguang Chemical Group) with block copolymer P123 ($EO_{20}PO_{70}EO_{20}$, Sigma–Aldrich) as a templating agent. In a typical synthesis, 0.67 g of P123, 1.21 g of NaCl, and 0.20 mL of $NH_4F$ solution (0.25 M) were mixed with 20.8 mL of HCl solution of varying concentration (0, $1\times10^{-3}$, $5\times10^{-3}$, and $1\times10^{-2}$ M). The solution was stirred at 40 °C for 3 h. Then, a mixture of TMOS and **1** was added to above solution under vigorous stirring. The molar ratio between the different components is (TMOS+**1**)/$H_2O$/P123/$NH_4F$/NaCl/HCl = 1:163:0.016:0.007:2.945:(0–0.029). The resultant slurry was further stirred at 40 °C for 24 h and then aged at 80 °C for another 24 h. The as-synthesized product was recovered by filtration, washed with deionized water, and dried in air under ambient conditions. To extract the template, the as-synthesized solid was stirred in ethanol at reflux for 24 h, and then filtered, washed with ethanol, and dried in air.

*Epoxidation of Allyl Alcohol*

The conditions of the epoxidation experiment are similar to those in the previous report.[32] Titanium tetraisopropoxide (0.5 mmol, Sigma–Aldrich), the hybrid chiral material (with a molar ratio of tartardiamide to titanium of 1.5:1), and dry $CH_2Cl_2$ (20 mL) were added to a 50-mL Schlenk-type flask under argon. The mixture was cooled to 0 °C and stirred for 4 h. Allyl alcohol (10 mmol) and *n*-nonane (internal standard) were then added. *tert*-Butyl hydroperoxide (20 mmol, Fluka) in $CH_2Cl_2$ (5.5 M) was added dropwise with stirring. The mixture was stirred at 0 °C for 48 h. After the reaction, the solid material was filtered and the filtrate was analyzed by Agilent 6890 gas chromatography on a chiral β-cyclodextrin column.

*Characterization*

X-ray powder diffraction (XRD) patterns were recorded on a Rigaku D/Max 3400 powder diffraction system using $Cu_{K\alpha}$ radiation of wavelength 1.542 Å. The nitrogen sorption experiments were performed at 77 K on an ASAP 2000 system. Samples were degassed at 120 °C for 5 h prior to the measurements. BET surface area was calculated from the adsorption data in a relative pressure $P/P_0$ range from 0.04 to 0.2. Pore size distribution was determined from the adsorption branches using the Barret–Joyner–Halenda (BJH) method. Pore volume was estimated at a relative pressure $P/P_0$ of 0.99. Transmision electron microscopy (TEM) was performed using a JEM-2010 at an acceleration voltage of 200 kV. FTIR spectra were collected with a Nicolet Nexus 470 IR spectrometer with KBr pellet. $^{13}C$ (100.6 MHz) cross-polarization magic-angle spinning (CP-MAS) and $^{29}Si$ (79.5 MHz) MAS NMR experiments were recorded on a Bruker DRX-400 spectrometer equipped with a magic-angle spin probe in a 4-mm $ZrO_2$ rotor using tetramethylsilane as reference: for $^{13}C$ CP-MAS NMR experiments, 8 kHz spin rate, 3 s pulse delay, 4 min contact time, and 1000 scans; for $^{29}Si$ MAS NMR experiments, 8 kHz spin rate, 3 s pulse delay, 10 min contact time, and 1000 scans. CHN elemental analyses were determined on an Elementar Vario EL III. Thermal gravimetric analysis was performed with a Perkin–Elmer Pyris Diamond TG analyzer in a nitrogen atmosphere from room temperature to 900 °C with a heating rate of 10 °C $min^{-1}$. The optical activity was measured with JASCO P-1020, 5 s integration, 10 repeat times, 100 mm cell length. Before the measurement, 0.05 g of the material was dissolved in 10 mL of NaOH aqueous solution (1.0 M) at 10 °C.

  

## Acknowledgements

This work was supported by the National Natural Science Foundation of China (20621063, 20673113, 20703044) and the National Basic Research Program of China (2003CB615803).

[1] C. E. Song, S. Lee, *Chem. Rev.* **2002**, *102*, 3495–3524.
[2] C. Li, H. Zhang, D. Jiang, Q. Yang, *Chem. Commun.* **2007**, 547–558.
[3] C. Roussel, A. D. Rio, J. Pierrot-Sanders, P. Piras, N. Vanthuyne, *J. Chromatogr. A* **2004**, *1037*, 311–328.
[4] A. Kurganov, *J. Chromatogr. A* **2001**, *906*, 51–71.
[5] R. Lakes, *Int. J. Mech. Sci.* **2001**, *43*, 1579–1589.
[6] M. E. Davis, *Nature* **2002**, *417*, 813–821.
[7] Polarz, B. Smarsly, *J. Nanosci. Nanotechnol.* **2002**, *2*, 581–612.
[8] G. J. de A. A. Soler-Illia, C. Sanchez, B. Lebeau, J. Patarin, *Chem. Rev.* **2002**, *102*, 4093–4138.
[9] S. Inagaki, S. Guan, Y. Fukushima, T. Ohsuna, O. Terasaki, *J. Am. Chem. Soc.* **1999**, *121*, 9611–9614.
[10] B. J. Melde, B. T. Holland, C. F. Blanford, A. Stein, *Chem. Mater.* **1999**, *11*, 3302–3308.
[11] T. Asefa, M. J. MacLachlan, N. Coombs, G. A. Ozin, *Nature* **1999**, *402*, 867–871.
[12] B. Haton, K. Landskron, W. Whitnall, D. Perovic, G. A. Ozin, *Acc. Chem. Res.* **2005**, *38*, 305–312.
[13] F. Hoffmann, M. Cornelius, J. Morell, M. Fröba, *J. Nanosci. Nanotechnol.* **2006**, *6*, 265–288.
[14] C. Yoshina-Ishii, T. Asefa, N. Coombs, M. J. MacLachlan, G. A. Ozin, *Chem. Commun.* **1999**, 2539–2540.
[15] G. Dubois, R. J. P. Corriu, C. Reyé, S. Brandès, F. Denat, R. Guilard, *Chem. Commun.* **1999**, 2283–2284.
[16] K. Landskron, G. A. Ozin, *Science* **2004**, *306*, 1529–1532.
[17] L. Zhang, H. C. L. Abbenhuis, Q. H. Yang, Y.-M. Wang, P. C. M. M. Magusin, B. Mezari, R. A. van Santen, C. Li, *Angew. Chem.* **2007**, *119*, 5091–5094; *Angew. Chem. Int. Ed.* **2007**, *46*, 5003–5006.
[18] M. J. MacLachlan, T. Asefa, G. A. Ozin, *Chem. Eur. J.* **2000**, *6*, 2507–2511.
[19] S. Polarz, A. Kuschel, *Adv. Mater.* **2006**, *18*, 1206–1209.
[20] A. Ide, R. Voss, G. Scholz, G. A. Ozin, M. Antonietti, A. Thomas, *Chem. Mater.* **2007**, *19*, 2649–2657.
[21] S. Inagaki, S. Guan, Q. H. Yang, M. P. Kapoor, T. Shimada, *Chem. Commun.* **2008**, 202–204.
[22] C. Baleizão, B. Gigante, D. Das, M. Álvaro, H. García, A. Corma, *Chem. Commun.* **2003**, 1860–1861.
[23] C. Baleizão, B. Gigante, D. Das, M. Álvaro, H. García, A. Corma, *J. Catal.* **2004**, *223*, 106–113.
[24] M. Álvaro, M. Benitez, D. Das, B. Ferrer, H. García, *Chem. Mater.* **2004**, *16*, 2222–2228.
[25] M. Benitez, G. Bringmann, M. Dreyer, H. García, H. Ihmels, M. Waidelich, K. Wissel, *J. Org. Chem.* **2005**, *70*, 2315–2321.
[26] D. M. Jiang, Q. H. Yang, H. Wang, G. Zhu, J. Yang, C. Li, *J. Catal.* **2006**, *239*, 65–73.
[27] Y. Wan, Y. Shi, D. Zhao, *Chem. Commun.* **2007**, 897–926.
[28] D. Zhao, Q. Huo, J. Feng, B. F. Chmelka, G. D. Stucky, *J. Am. Chem. Soc.* **1998**, *120*, 6024–6036.
[29] J. M. Kim, Y.-J. Han, B. F. Chmelka, G. D. Stucky, *Chem. Commun.* **2000**, 2437–2438.
[30] L. Padmaja, T. Vijayakumar, I. Hubert Joe, C. P. Reghunadhan Nair, V. S. Jayakumar, *J. Raman Spectrosc.* **2006**, *37*, 1427–1441.
[31] S. S. Woodard, M. G. Finn, K. B. Sharpless, *J. Am. Chem. Soc.* **1991**, *113*, 106–113.
[32] S. Xiang, Y. L. Zhang, Q. Xin, C. Li, *Angew. Chem.* **2002**, *114*, 849–852; *Angew. Chem. Int. Ed.* **2002**, *41*, 821–824.
[33] P. Pitchen, H. B. Kagan, *Tetrahedron Lett.* **1984**, *25*, 1049–1052.
[34] G. P. Webb, B. Wells, *Catal. Today* **1992**, *12*, 319–337.
[35] Y. Dobashi, S. Hara, *J. Org. Chem.* **1987**, *52*, 2490–2496.
[36] S. G. Allenmark, S. Andersson, P. Möller, D. Sanchez, *Chirality* **1995**, *7*, 248–256.
[37] S. S. Kim, A. Karkamkar, T. J. Pinnavaia, M. Kruk, M. Jaroniec, *J. Phys. Chem. B* **2001**, *105*, 7663–7670.
[38] C. Yu, B. Tian, J. Fan, G. D. Stucky, D. Zhao, *Chem. Commun.* **2001**, 2726–2727.
[39] S. A. Bagshaw, E. Prouzet, T. J. Pinnavaia, *Science* **1995**, *269*, 1242–1244.
[40] P. Ågren, M. Lindén, J. B. Rosenholm, R. Schwarzenbacher, M. Kriechbaum, H. Amenitsch, P. Laggner, J. Blanchard, F. Schüth, *J. Phys. Chem. B* **1999**, *103*, 5943–5948.
[41] M. Impéror-Clerc, P. Davidson, A. Davidson, *J. Am. Chem. Soc.* **2000**, *122*, 11925–11933.
[42] A. F. Gross, V. H. Le, B. L. Kirsch, A. E. Riley, S. H. Tolbert, *Chem. Mater.* **2001**, *13*, 3571–3579.
[43] X. Y. Bao, X. S. Zhao, X. Li, P. A. Chia, J. Li, *J. Phys. Chem. B* **2004**, *108*, 4684–4689.

Received: April 7, 2008
Published online: June 24, 2008

  